HHS Public Access

Author manuscript

Traffic. Author manuscript; available in PMC 2018 December 01.

Published in final edited form as:

Traffic. 2017 December ; 18(12): 776–790. doi:10.1111/tra.12526.

Nup42 and IP_6 coordinate Gle1 stimulation of Dbp5/DDX19B for mRNA export in yeast and human cells

Rebecca L. Adams, **Aaron C. Mason**, **Laura Glass**, **Aditi**, and **Susan R. Wente**[1]

Department of Cell and Developmental Biology, Vanderbilt University School of Medicine, Nashville, TN 37240-7935

Abstract

The mRNA lifecycle is driven through spatiotemporal changes in the protein composition of mRNA particles (mRNPs) that are triggered by RNA-dependent DEAD-box protein (Dbp) ATPases. As mRNPs exit the nuclear pore complex (NPC) in *Saccharomyces cerevisiae*, this remodeling occurs through activation of Dbp5 by inositol hexakisphosphate (IP_6)-bound Gle1. At the NPC, Gle1 also binds Nup42, but Nup42's molecular function is unclear. Here we employ the power of structure-function analysis in *S. cerevisiae* and human (h) cells, and find that the high-affinity Nup42-Gle1 interaction is integral to Dbp5 (hDDX19B) activation and efficient mRNA export. The Nup42 carboxy-terminal domain (CTD) binds Gle1/hGle1B at an interface distinct from the Gle1-Dbp5/hDDX19B interaction site. A nup42-CTD/gle1-CTD/Dbp5 trimeric complex forms in the presence of IP_6. Deletion of *NUP42* abrogates Gle1-Dbp5 interaction, and disruption of the Nup42 or IP_6 binding interfaces on Gle1/hGle1B leads to defective mRNA export in *S. cerevisiae* and human cells. *In vitro*, Nup42-CTD and IP_6 stimulate Gle1/hGle1B activation of Dbp5 and DDX19B recombinant proteins in similar, non-additive manners, demonstrating complete functional conservation between humans and *S. cerevisiae*. Together, a highly conserved mechanism governs spatial coordination of mRNP remodeling during export. This has implications for understanding human disease mutations that perturb the Nup42-hGle1B interaction.

Phrases

nuclear pore complex; mRNA export; Gle1; Dbp5; Nup42; inositol hexakisphosphate; mRNP remodeling

INTRODUCTION

Eukaryotic cellular function is dependent on the proper and efficient export of mRNAs from the nucleus through nuclear envelope (NE)-embedded NPCs to the cytoplasm. An essential rate-limiting step in this pathway occurs at the cytoplasmic face of the NPC on a structural platform over the NPC central channel[1,2]. At this site, the ATPase cycle of the *S. cerevisiae*

[1]Corresponding Author: Susan R. Wente, Ph. D., Department of Cell and Developmental Biology, Vanderbilt University School of Medicine, 3140A MRBIII, Nashville, TN 37240-7935, Telephone: (615) 322-4219, Fax: (615) 343-8340, susan.wente@vanderbilt.edu.

The authors declare no competing financial interests.

Dbp5 (DDX19B in human) mediates release of the export factor Mex67-Mtr2 (NXF1 in human) and other RNA-binding proteins (RBPs) from the translocating mRNPs[3,4]. Several essential factors regulate the Dbp5 ATPase cycle at the NPC cytoplasmic face: the nucleoporin Nup159 (Nup214 in human) which facilitates ADP release[5], and the protein Gle1 bound to IP_6 which enhances ATP loading for triggering RNA-dependent ATP hydrolysis[5–8]. Control of the Dbp5 ATPase by Gle1-IP_6 and Nup159 at the NPC cytoplasmic face results in spatially coordinated mRNP remodeling of Mex67-Mtr2 and RBPs from exporting mRNPs. As such, directionality is conferred on the export mechanism, allowing release of the mRNP to the cytoplasm for protein synthesis.

Although first identified as an NPC-associated mRNA export factor in *S. cerevisiae*[9], Gle1 is conserved in higher eukaryotes[10,11]. In addition to regulating Dbp5 at the NPC, Gle1 is required for the function of distinct Dbps at non-NPC subcellular locales. In *S. cerevisiae*, Gle1-IP_6 regulates Dbp5 activity during translation termination, and Gle1 impacts the ATPase activity and RNA binding of Ded1, another DEAD-box protein, for efficient translation initiation independently of IP_6[12–15]. In humans, hGle1 shuttles between the nucleus and cytoplasm with at least two isoforms, hGle1A and hGle1B, produced from a single gene[11,16]. hGle1A and hGleB are identical except for the C-terminal region wherein differential splicing results in an extended 43 amino acids in hGle1B (Figure 1A)[16]. The hGle1B isoform localizes predominantly at the NPC and is required for mRNA export[16,17] whereas hGle1A is not functional at the NPC and has cytoplasmic roles at stress granules and in regulating the human Ded1 homologue DDX3 during translation[18]. Most recently, hGle1 has also been implicated in centrosome assembly and cilia function, potentially regulating an unidentified DEAD-box protein for localized mRNA metabolism[19]. Taken together, Gle1 and hGle1 play critical roles in regulating Dbps during multiple stages in gene expression at distinct subcellular locations.

It is speculated that Gle1's multi-functional capabilities are dictated by unique protein interaction partners at different subcellular sites[20]. Thus, to understand how spatial regulation of Dbp5 is controlled at the NPC cytoplasmic face, it is important to precisely pinpoint the roles of Gle1 interactions at the NPC. The amino terminal half of Gle1 contains a coiled-coil region that promotes Gle1 self-association and is required for NPC localization (Figure 1A)[17]. Intriguingly, this region of Gle1 crosslinks to several members of the Nup82 holo-complex[1], suggesting a potential mechanism for Gle1 localization at the NPC through direct interaction with this cytoplasmically-oriented complex. The region comprising the first 29 amino acids of the human Gle1 amino-terminus also binds to human Nup155, and is required for NPC localization (Figure 1A)[21]. Finally, the carboxy-terminal domain (CTD) of Gle1/hGle1B binds the CTD of Nup42/hNup42 (also known as Rip1 in *S. cerevisiae* and hCG1 or NUPL2 in human) (Figure 1B)[9,22,23]. The recent structural model of the cytoplasmic NPC face proposes that Gle1, Dbp5, and Nup42 are possibly oriented toward the NPC central channel[1], positioning these factors for interaction with exporting mRNPs. However, the molecular details of the interactions that allow this Gle1 positioning are still undetermined. Revealing how Gle1 acts at the NPC is also needed to give insight into human disease mechanisms. Disease mutations linked to *hGLE1* that alter hGle1 self-association, the hGle1-hNup42 interaction, and/or the respective pools of hGle1 at the NPC versus in the

cytoplasm are associated with devastating pathologies including lethal congenital contracture syndrome 1 (LCCS1)[17,24,25] and amyotrophic lateral sclerosis (ALS)[26,27].

With respect to Nup42, some discrete functions at the NPC have been defined for its different domains. Our prior studies revealed a role for the FG domain in recruiting the mRNP to be in proximity to Gle1 and Dbp5 for remodeling[28], via the Nup42 FG domain interacting with Mex67-Mtr2 (Figure 1B)[29]. In fact, a fusion between Gle1 and the FG domain of Nup42 (gle1-FG^{nup42}) bypasses the requirement for Nup42 in some genetic contexts[28]. The Nup42 CTD is also required for specific functions. Nup42/hNup42 mediates the export of heat shock transcripts[22,30], and deletion of *NUP42* together with *IPK1*, the kinase that produces IP_6, results in a temperature sensitive mRNA export defect[31]. Nup42 CTD expression is sufficient for the function in heat shock mRNA export[32] and rescues *nup42Δ ipk1Δ* temperature sensitivity[31]; whereas, expression of the gle1-FG^{nup42} fusion does not restore these defects in *nup42Δ*mutants[28]. Since proper Gle1 and Dbp5 function are likewise required for heat shock mRNA export[30,33], and IP_6 is required for normal Gle1 regulation of Dbp5, we propose that the Nup42 CTD might also impact their interaction.

Nup42 was among the first identified NPC constituents[34], but molecular details of its role at the NPC remain unresolved. Current models propose that the Nup42 CTD serves as a docking site for Gle1 at the NPC, and hNup42 for hGle1B. However, hGle1A lacks efficient binding to hNup42 but localizes to the NPC upon *hGLE1* knockdown[18,22]. More importantly, cells with only hGle1A at the NPC are defective for mRNA export[18]. Thus, Gle1 interaction with Nup42 might be required for proper Gle1 function beyond any role in NPC localization. To further define the mRNA export mechanism mediated by the Gle1-Nup42 interaction at the NPC, we conducted a series of biochemical, genetic and cell biological studies with both the *S. cerevisiae* and human proteins and respective cells. We find here that Nup42/hNup42 and IP_6 have conserved functions in enhancing Gle1/hGle1B stimulation of Dbp5/DDX19B for mRNA export.

RESULTS

Gle1-Nup42 interaction is required for heat shock mRNA export

To further investigate the Gle1-Nup42 function, we used a structural homology approach to pinpoint residues critical for the interaction. Gle1/hGle1B binding to Nup42/hNup42 is so highly conserved that the hNup42 CTD interacts with *S. cerevisiae* Gle1 and rescues the heat shock mRNA export defect of *nup42Δ* mutants[23]. Thus, we hypothesized that the amino acid residues involved in the Gle1/hGle1B-Nup42/hNup42 interaction are conserved. From a Clustal Omega[35] alignment between *S. cerevisiae* Gle1 and hGle1B, we mapped the conserved human residues onto the *S. cerevisiae* protein structure of gle1^{H337R}-IP_6-dbp5^{L327V}, PDB 3RRM[7]). A patch of conserved residues was apparent on the surface of Gle1 that was distinct from the Dbp5 binding interface (Figure 1C). Four polar residues were surface accessible on this patch: Q491, K494, E501, and E502 (Figure 1D). We altered these residues to alanine, first as pairs, then all together, and analyzed the interaction with nup42-CTD via the yeast two-hybrid assay (Y2H). Strains expressing each of the pairwise *gle1* mutants (*GBD-gle1-CTD$^{QK>AA}$* and *GBD-gle1-CTD$^{EE>AA}$*) showed growth with *GAD-nup42-CTD*, but altering all four residues (*GBD-gle1-CTD$^{QKEE>AAAA}$*) resulted in no

growth on quadruple dropout media, indicating defective interaction with GAD-nup42-CTD (Figure 2A).

Next, we analyzed the function of *gle1*$^{QKEE>AAAA}$ *in vivo*. The altered proteins were expressed similar to wild-type Gle1 levels (Figure S1A), rescued a *gle1Δ* mutant, and displayed no obvious growth defects at all temperatures analyzed, similar to the growth of *nup42Δ* (Figure 2B, top panel). When expressed as the only copy in cells (Figure S1B), GFP-tagged gle1$^{QKEE>AAAA}$ localized at the NE rim to the same relative extent as wild-type Gle1-GFP. Similarly, Gle1-GFP was localized to the NE rim in *nup42Δ* cells (Figure 2C). However, *gle1*$^{QKEE>AAAA}$ mutants demonstrate a temperature-sensitive growth defect when combined with *ipk1Δ* mutants, phenocopying the growth defect previously observed with *nup42Δ ipk1Δ* mutants (Figure 2B, bottom panel)[31]. Finally, we analyzed heat shock mRNA export by testing^{35}S methionine incorporation to protein synthesis after shifting to growth at 42°C. Under these conditions, poly (A)$^{+}$ RNA is retained in the nucleus, but heat shock transcripts are permitted to export, resulting in preferential translation of heat shock proteins[36]. Previous analysis had determined that *nup42Δ* mutants are defective in heat shock mRNA export and protein production[30,32], so we anticipated that loss of nup42 binding by the gle1$^{QKEE-AAAA}$ protein would likewise impact the heat shock response. Indeed, the *gle1*$^{QKEE>AAAA}$ mutant demonstrated a loss of heat shock protein production similar to *nup42Δ* mutants (Figure 2D, lanes 8, 10). Therefore, we concluded that the Gle1-Nup42 interaction is required for heat shock mRNA export, gle1$^{QKEE>AAAA}$ disrupts this interaction, and association with Nup42 is not required for Gle1 localization at the NPC.

A minimal region of Nup42 that binds Gle1 is not sufficient for function

Prior studies defined the Nup42 CTD (residues 365–430) as sufficient for Y2H interaction with Gle1[23]. Using XtalPred-RF[37], the Nup42 CTD was predicted to have significant regions of disorder (data not shown). To more narrowly define the required Gle1 interaction domain in the Nup42 CTD, we generated a series of nup42-CTD truncations in the Y2H bait construct (*GAD-nup42-CTD*) and assayed with *GBD-gle1-CTD*. Both the *GAD-nup42*$^{405–424}$ and *GAD-nup42*$^{408–425}$ strains showed growth with *GBD-gle1-CTD*, revealing a region of seventeen residues (408–424) as necessary for the Gle1-Nup42 interaction (Figure 3A). Moreover, *GAD-nup42* truncations lacking residues 408–424 did not grow with *GBD-gle1-CTD*. From a Clustal Omega alignment of nup42-CTD and hnup42-CTD, residues 408–424 were in the most highly conserved region (Figure 3B). Observing conservation in the minimal Nup42 region required for Nup42-Gle1 binding is consistent with the fact that altering residues found on the conserved patch Gle1 disrupts interaction with Nup42 (Figure 2). BioLayer Interferometry analysis demonstrated a high affinity interaction between recombinant purified MPB-gle1-CTD and a biotinylated peptide corresponding to nup42$^{408–424}$, with a K_D of 0.0915 μM (Figure 3C). Purified recombinant MBP-gle1-CTD$^{QKEE>AAAA}$ had significantly reduced association with the biotin-nup42$^{408–424}$ peptide with a K_D of 0.599 μM. Thus, the nup42$^{408–424}$ region was necessary and sufficient for physically binding Gle1.

To determine whether this nup42$^{408–424}$ motif was sufficient for NE rim localization, GFP-tagged Nup42 proteins were expressed in *nup42Δ* and *gle1*$^{QKEE>AAAA}$ *nup42Δ* cells.

Direct fluorescence microscopy showed full-length GFP-Nup42 and GFP-nup42-CTD both localized comparably at the NE rim, indicative of NPC incorporation (Figure 3D). Although a higher background of pan-cellular signal was observed, GFP-nup42$^{408–424}$ also localized to the NE rim, and, importantly, GFP-nup42$^{408–424}$ localization was absent from the NE in *gle1$^{QKEE>AAAA}$* mutant cells (Figure 3D). This suggested that interaction with Gle1 is sufficient for localizing GFP-nup42$^{408–424}$ to the NPC. However, GFP-Nup42 and GFP-nup42-CTD were NE rim-localized in *gle1$^{QKEE>AAAA}$* mutants, indicating that additional NPC interactions besides Gle1 contribute to Nup42 localization. Interestingly, Nup42 proteins lacking the Gle1 interaction site (GFP-nup42Δ408–424 and GFP-nup42-CTDΔ408–424) were not detected by fluorescence microscopy or immunoblotting, suggesting that loss of interaction with Gle1 reduces Nup42 stability (Figure S2B).

Because nup42$^{408–424}$ bound Gle1 and localized to the NE rim, we speculated that the nup42$^{408–424}$ minimal domain might also be sufficient for functions attributed to the Nup42 CTD. Genetic tests were conducted to determine whether expression of *nup42$^{408–424}$* alone could rescue defects associated with absence of the Nup42 CTD. Centromeric *GFP-NUP42*, *GFP-nup42-CTD*, *and GFP-nup42$^{408–424}$* expression vectors were transformed into the temperature sensitive *nup42Δ ipk1Δ* mutant and growth was assessed at various temperatures. Similar to previously published results[31], *GFP-NUP42* and *GFP-nup42-CTD* rescued the temperature-sensitivity of *nup42Δ ipk1Δ*. However, *GFP-nup42$^{408–424}$* did not rescue the growth defects (Figure 3E; land 6, 8). The Nup42 CTD is also required for export of heat-shock transcripts following a temperature shift to 42°C[23]. Therefore, we tested whether *GFP-nup42$^{408–424}$* cells produced heat shock proteins as an assay for heat-shock mRNA export. Although *GFP-nup42-CTD* cells produced heat-shock proteins, *GFP-nup42$^{408–424}$* cells did not (Figure 3F). Untagged *nup42$^{408–424}$* also did not rescue *nup42Δ* growth and heat-shock mRNA export defects (data not shown). Thus, although nup42$^{408–424}$ was sufficient for interaction with Gle1 and localization to the NE, this region was not sufficient to rescue the function of the Nup42 CTD.

Nup42 interacts with IP$_6$-Gle1-Dbp5 complexes

The Gle1 CTD interacts with both Nup42 and Dbp5 and our mutation analysis indicated that Nup42 and Dbp5 interact at distinct Gle1 interfaces. To reveal the role of the Nup42 CTD, we tested whether Gle1 can simultaneously bind both Nup42 and Dbp5. Soluble binding assays were performed with purified recombinant proteins. We used the gain-of-function proteins MBP-gle1-CTD^{H337R} and/or dbp5^{L327V} from prior structural studies[7] and GST or GST-nup42-CTD bound to resin. A trimeric GST-nup42-CTD/MPB-gle1-CTD^{H337R}/dbp5^{L327V} complex was observed only in the presence of IP$_6$ (Figure 4A; lane 13, 14). In this assay, binding of GST-nup42-CTD to dbp5^{L327V} was not observed in the absence of MBP-gle1^{-}CTD^{H337R} (Figure 4A; lane 11, 14). Thus, Gle1 bound Nup42, Dbp5, and IP$_6$ at the same time forming an IP$_6$-trimeric protein complex.

To investigate whether Nup42 impacts the interaction between wild-type Gle1 and Dbp5 in cells, we used the Y2H assay. Notably, although *GAD-DBP5* and *GBD-gle1-CTD* cells grew on selective media, *GAD-DBP5* and *GBD-gle1-CTD$^{QKEE>AAAA}$* cells did not (Figure 4B). Thus, in the Y2H assay, Nup42 interaction was required for Gle1 to bind Dbp5. As a further

test of this, we compared Y2H results in a reporter strain with *NUP42* deleted. The *nup42Δ* reporter strain expressing *GAD-DBP5* and *GBD-gle1-CTD* did not grow (Figure 4C). Notably, the *GBD-gle1-CTD*$^{VAI>DDD}$ mutant (shown previously to disrupt Gle1 stimulation of Dbp5[7]) also did not interact with *GAD-DBP5* by Y2H (Figure 4B), even though *GBD-gle1-CTD*$^{VAI>DDD}$ did grow with *GAD-nup42-CTD* (Figure 2A). These results provided further support that Gle1 binds Nup42 and Dbp5 at different interfaces and that Nup42 might impact the interaction between Gle1 and Dbp5.

Gle1 stimulation of Dbp5 ATPase activity is enhanced by Nup42 or IP_6

To directly determine whether Nup42 CTD has an effect on Gle1 stimulation of the RNA-dependent Dbp5 ATPase activity, *in vitro* assays were conducted using our established methods and bacterially-expressed recombinant proteins (Figure 4D). Upon addition of IP_6, Gle1 stimulates the ATPase activity of Dbp5 ~6-fold in a colorimetric enzyme coupled ATPase rate assay (Figure 4E; lane 2, 7, 8), as previously determined[6,8]. Under these conditions, when recombinant purified H_6-nup42-CTD was added at 750nM into the assay, no obvious change in ATPase activity was observed (Figure 4E, lane 12). Because our hypothesis is that Nup42 enhances the interaction between Gle1 and Dbp5, and IP_6 performs a similar function[6,8], we then tested whether H_6-nup42-CTD affected the Dbp5 ATPase activity in the absence of IP_6. Indeed, dose-dependent enhancement of gle1-CTD -stimulated Dbp5 ATPase activity was observed when H_6-nup42-CTD was added to this assay without IP_6 present (Figure 4E, lanes 9–11). Of note, the full Nup42 CTD (residues 365–430) was required for this stimulation as the nup42$^{408–424}$ peptide did not enhance ATPase activity when titrated at the same molar concentrations (Figure 4E, lanes 19–21). H_6-nup42-CTD did not stimulate Dbp5 ATPase activity in the absence of gle1-CTD (data not shown). Finally, although gle1-CTD$^{QKEE>AAAA}$ showed somewhat reduced stimulation of Dbp5 in the presence of IP_6 (Figure 4E; lane 8, 14), H_6-nup42-CTD demonstrated no dose-dependent enhancement of Dbp5 ATPase activity in the presence of gle1-CTD$^{QKEE>AAAA}$. Therefore, through interaction with Gle1, Nup42 and IP_6 each augmented Gle1-mediated stimulation of Dbp5 in manners that were not additive.

The hNup42-hGle1B interaction is conserved in human cells and required for mRNA export

Because the QKEE residues for Nup42 interaction in *S. cerevisiae* Gle1 are conserved in hGle1B (Figure 1D), we investigated whether hGle1B requires hNup42 interaction in a similar manner. We first examined the localization of mCherry-hGle1B and mCherry-hgle1B$^{QKED>AAAA}$ in HeLa cells. Although mCherry-hgle1B$^{QKED>AAAA}$ was expressed at lower levels than mCherry-hGle1B (Figure S3A), mCherry-hgle1B$^{QKED>AAAA}$ was detected at the NE rim in a subset of transfected cells (Figure 5A). More importantly, the proportion of cells exhibiting NE-localized mCherry-hgle1B$^{QKED>AAAA}$ increased upon siRNA-mediated *hGLE1* knockdown (Figure 5B), indicating that endogenous hGle1 outcompetes hgle1B$^{QKED>AAAA}$ for NE rim localization. This is identical to hGle1A behavior wherein it only localizes at the NE rim in the absence of hGle1B[18]. To analyze whether mCherry-hgle1B$^{QKED>AAAA}$ was functional for mRNA export, we tested for complementation of the mRNA export defect upon *hGLE1* knock down (Figure S3B). As previously demonstrated[17], knockdown of *hGLE1* (A and B) with specific siRNAs resulted in accumulation of poly(A)$^+$ RNA in the nucleus, and expression of siRNA-resistant

mCherry-hGLE1B^{R} rescued the mRNA export defect (Figure 5C, 5D). However, expression of siRNA-resistant *mCherry-hgle1B*$^{R\ QKED>AAAA}$ did not rescue of mRNA export. No change in the nuclear:cytoplasmic ratio of poly(A)$^{+}$ RNA was observed in *mCherry-hgle1B*$^{R\text{-}QKED>AAAA}$ transfected cells, compared to vehicle and *mCherry* (Figure 5D). Indeed, cells with rim-localized mCherry-hgle1B$^{QKED>AAAA}$ maintained a significant mRNA export defect (Figure 5C). These results indicated that the conserved QKED residues are required for hGle1B function, suggesting that interaction with hNup42 is required for mRNA export in human cells.

hNup42 is required for human mRNA export

Prior studies by our laboratory and others tested for roles of the human homologues of *S. cerevisiae* Gle1, Dbp5, and Ipk1 in mRNA export through NPCs. Knockdown of *hGLE1B*, *DDX19B*, and *hIPK1* (also known as IPPK) or dominant negative functional perturbation results in nuclear accumulation of poly(A)$^{+}$ RNA[16,17,38,39], reflecting a block to mRNA export. Although we previously showed that hNup42 is required for heat-shock mRNA export[22], mRNA export under normal growth conditions was not assessed. To test this directly, siRNA knockdown of *hNUP42* in HeLa cells was conducted and poly(A)$^{+}$ RNA localization analyzed at 37°C. A robust nuclear accumulation of poly(A)$^{+}$ RNA signal, with loss of cytoplasmic signal, was observed when hNup42 was depleted (Figures 5E, S3C). Quantification demonstrated a statistically significant increase in the nuclear:cytoplasmic signal for poly(A)$^{+}$ RNA upon *hNUP42* knockdown (Figure 5F). Therefore, hNup42 was essential for mRNA export in human cells, corroborating the mRNA export defect observed in *mCherry-hgle1B*$^{R\text{-}QKED>AAAA}$ cells. Further, as depletion of each of the factors all result in mRNA export defects, we concluded that the molecular mechanism for human hGle1B, DDX19B, hNup42, and IP_6 function in mRNA export is similar to that of their *S. cerevisiae* homologues.

hNup42 and IP_6 each enhance hGle1B stimulation of DDX19B ATPase activity

To further examine the conservation of hNup42 and IP_6 functions in the human system, direct *in vitro* ATPase assays were conducted with DDX19B. Initial experiments were performed with purified bacterially-expressed DDX19B (denoted DDX19B*) (Figure S4); however, the bacterially-expressed DDX19B* with or without hgle1B-CTD had ~8.3 fold lower enzymatic activity compared to that of *S. cerevisiae* Dbp5, gle1-CTD and IP_6 (Figure S4). We then tested His-tagged DDX19B (H_6-DDX19B) purified from a Baculoviral expression system in insect cells based on reported successful DDX19B *in vitro* protein interaction studies and reports that DDX19B is post-translationally modified in mammalian cells[40,41] (Figure 6A), The H_6-DDX19B purified from insect cells displayed significant ATPase activity which was stimulated ~4-fold by hgle1B-CTD in the presence of IP_6 (Figure 6B; lane 2, 6, 7). Strikingly, titration of hnup42-CTD resulted in dose-dependent enhancement of the hGle1B-stimulated H_6-DDX19B ATPase activity in the absence of IP_6 (Figure 6B, lanes 8–10). hNup42 and IP_6 did not have an additive effect (Figure 6B; lanes 7, 10, 11). Finally, although IP_6 further stimulated the hgle1B$^{QKED>AAAA}$ mediated activation of H_6-DDX19B (Figure 6B; lane 12, 13), hnup42-CTD did not enhance hgle1B$^{QKED>AAAA}$ stimulation of H_6-DDX19B ATPase activity (Figure 6B, lanes 14–16). In sum, *in vitro*

human DDX19B activation was dependent on IP_6, hGle1B, and hNup42, with the human and *S. cerevisiae* proteins showing fully conserved *in vitro* functions.

hGle1B requires conserved IP_6 binding residues for DDX19B stimulation and mRNA export

To further investigate the IP_6 dependence of hGle1B-DDX19B activity in human cells, we tested whether hGle1B coordinates IP_6 through the same surface accessible protein interface as the *S. cerevisiae* Gle1. We previously defined the residues required for IP_6 binding to *S. cerevisiae* Gle1 (K377 and K378) by identification of positive residues that were conserved across fungal and metazoan species[10]. In prior structural modeling of fungal, plant and human Gle1, it was observed that the IP_6 binding pocket of hGle1 and *Arabidopsis thaliana* Gle1 is less positively-charged than that of *S. cerevisiae*[42]. However, the homologous IP_6-coordinating lysine (K) residues of hGle1B (K526, K527) are conserved. Altering these lysine (K) residues of hGle1B (K526, K527) to glutamine (Q) (hgle1B-CTD$^{KK>QQ}$) abolished the enhanced stimulation of H_6-DDX19B in the presence of IP_6 (Figure 6C, comparing lanes 7, 10). We also tested a hGle1B variant with changes in two additional positively-charged residues (K479, K486) whose homologous residues are found near the IP_6 binding pocket of *S. cerevisiae* Gle1. The hgle1B-CTD$^{KKKK>QQQQ}$ also did not show IP_6 dependent stimulation of H_6-DDX19B. Importantly, the hgle1B-CTD$^{KK>QQ}$ protein still stimulated H_6-DDX19B at a basal level (Figure 6C, comparing lane 1 with 10 and 11), and with the addition of hnup42-CTD, hgle1B-CTD$^{KK>QQ}$ enhanced H_6-DDX19B ATPase activity levels comparable to that with wild-type hgle1B-CTD and hnup42-CTD (Figure 6C, lanes 12–14). Thus, the IP_6 interface changes on hgle1B-CTD$^{KK>QQ}$ did not perturb the hNup42 interface or overall folding.

Further supporting a conserved role for an IP_6 interaction with hGle1B during mRNA export, we found that expression of the siRNA-resistant GFP-hgle1B$^{KK>QQ}$ did not rescue the mRNA export defect seen with siRNA *hGLE1*-knockdown in human cells, whereas wild-type GFP-hGle1B did rescue (Figure 6D). As such, mRNA export was inhibited in human cells when the IP_6-dependent hGle1B function was perturbed by altering the conserved K526 and K527 residues. Thus, although the plant and human IP_6 interactions surfaces are less positively charged compared to *S. cerevisiae* and not fully homologous in terms of protein sequence, these results with the prior studies[42] documented a conserved requirement for IP_6 during hGle1B function in mRNA export in all tested eukaryotic cells.

DISCUSSION

Here we reveal important insights into the functional organization of the mRNA export machinery at the NPC cytoplasmic face. Our biochemical and physiological assays demonstrate a unique role for Nup42 in mediating Gle1 regulation of the Dbp5 ATPase activity. In both *S. cerevisiae* and human systems, Nup42 is not critical for localizing Gle1 at the NPC. Rather, Nup42/hNup42 enhances the Gle1/hGle1B stimulation of the RNA-dependent Dbp5/DDX19B ATPase (Figure 4E and 6B). We find that Gle1 utilizes distinct surface accessible binding sites for interaction with IP_6, Nup42 and Dbp5 (Figure 1C), and a nup42-CTD/gle1-CTD/Dbp5 trimeric complex forms in the presence of IP_6. As some of the *hGLE1* disease-associated mutations alter the carboxy-terminal region of hGle1B required

for hNup42 binding (Figure 1A)[25,27], we predict that perturbed DDX19B activation and mRNP remodeling dynamics at the NPC underlie some of these human pathologies.

An active role for Nup42 and hNup42 during mRNA export is distinct from the historically attributed function of these proteins in localizing Gle1/hGle1 to the NPC. Here, in *nup42Δ* mutants, we find Gle1-GFP localizes to the NPC as robustly as in wild-type cells, and *GFP-gle1*$^{QKEE>AAAA}$ is also localized to the NE rim (Figure 2C). In fact, Nup42 is at least partly reliant on Gle1 for its localization since GFP-nup42$^{408–424}$ is lost from the rim in *gle1*$^{QKEE>AAAA}$ mutants (Figure 3D). Moreover, the hGle1A isoform which lacks hNup42 binding localizes to the NPC in the absence of hGle1B[18], and hGle1 remains localized to the NE rim upon *hNUP42* knockdown[22]. A recent structural analysis of the Nup82 complex (Nup159, Nup82, Nsp1) revealed the interactions that anchor this complex to the *S. cerevisiae* NPC cytoplasmic side[1], with the FG domains for Nup159 and Nsp1 situated across the NPC channel for their function in mRNA export[28,43]. The Fernandez-Martinez study also reports substantial interactions between the Gle1 amino terminal region (NTD) and the Nup82 complex, which corroborates our prior finding that the hGle1 NTD is required for NPC localization (both its coiled-coil region and the Nup155 interaction region (Figure 1A,[17,21];. This also explains why overexpression of *GLE1* rescues growth defects of *nup82* mutants[44]. In contrast, Nup42's only reported crosslinking partner is Gle1[1]. Thus, the Gle1 NTD is the primary determinant of NPC localization whereas the Gle1 CTD interaction with Nup42 and IP_6 is required for mRNP remodeling.

Importantly, although a minimal conserved peptide of seventeen amino acids in Nup42 (nup42$^{408–424}$) is sufficient for interaction with Gle1, additional sequence in the Nup42 CTD is required for function (Figures 3, 4). A conserved patch on Gle1 is essential for interaction with the minimal nup42$^{408–424}$ peptide (Figure 1D, 2, 3), placing this interface at the opposite face of where Dbp5 binds Gle1 (Figure 1C,[7]). However, Nup42 is required for the Y2H interaction between Gle1 and Dbp5 in cells (Figure 4C). We predict that the sequence in the Nup42 CTD flanking the minimal Gle1 binding peptide (residues 408–424) is responsible for mediating the Gle1-Dbp5 interaction and the nup42-CTD/gle1-CTD activation of Dbp5. To date, we have not been able to determine whether this occurs directly (with Nup42 interacting with both Gle1 and Dbp5) or indirectly (with Nup42 binding Gle1 and altering its conformation). We did not observe a Nup42-Dbp5 interaction in our soluble binding assay (Figure 4A lane 11), but it is possible that low affinity interactions are not detected by this method. We also analyzed the IP_6-trimeric GST-nup42-CTD/MPB-gle1^{H337R}/dbp5^{L327V} protein complex formation in the presence of different nucleotides; however, no obvious differences in gle1^{H337R}-dbp5^{L327V} interaction were observed, potentially due to the use of gain-of-function proteins required for this assay (Figure 4A).

The hypothesis that Nup42 mediates an interaction between Gle1 and Dbp5 suggests that the Nup42 CTD role is similar to that of IP_6, explaining why no additive effect is seen with IP_6 and nup42-CTD during *in vitro* ATPase assays (Figure 4E and 6B). The redundant functions also explain why *nup42Δ ipk1Δ* double mutants are temperature-sensitive with no growth defects observed for single mutants in *S. cerevisiae*[31]. IP_6 is required for GST-nup42-CTD/MBP-gle1-CTD^{H337R}/dbp5^{L327V} trimeric protein complex formation in soluble binding assays (Figure 4A). We speculate that IP_6 is required *in vitro* for trimeric complex formation

but does not enhance Gle1 stimulation of Dbp5 in the presence of Nup42 because the former experiment requires capture of a stable interaction, whereas observation of ATPase activity only relies on transient stimulation. Having two parallel ways to support Gle1-Dbp5 interaction through either Nup42 or IP_6 potentially allows combinatorial control over the NPC-localized activity of Dbp5 in cells. Such spatial control is likely especially critical for modulating Gle1 through its multiple subcellular locations and functions.

We find that hGle1B, like *S. cerevisiae* Gle1, demonstrates enhanced stimulation of DDX19B in the presence of IP_6 or hNup42-CTD. However, in contrast to *S. cerevisiae*, hGle1B interactions with hNup42 and IP_6 are each individually required for mRNA export in human cells, indicating stricter control over this process *in vivo* (Figure 5 and 6D). The molecular requirement for hNup42 during nuclear mRNA export might also be due to the fact that the IP_6 binding pocket of hGle1B is less positively-charged[42] and potentially binds to IP_6 more weakly than *S. cerevisiae* Gle1 does to IP_6. However, as others have reported, the IP_6 binding pocket of *Arabidopsis thaliana* Gle1 has even lower positive charge than hGle1B but demonstrates enhanced stimulation of LOS4 (*A. thaliana* Dbp5 orthologue) in the presence of IP_6[42]. Therefore, a requirement for IP_6 in Gle1 stimulation of DEAD-box ATPases during mRNA export is conserved between *S. cerevisiae*, plants and human cells.

Based on our proposed mechanism for Nup42 CTD function, we posit that Nup42/hNup42 acts at an early step in the ATPase cycle of Dbp5/DDX19B at the NPC, where Gle1 enhances ATP loading onto Dbp5. This model is diagrammed in Figure 7. With the Nup42 FG domain recruiting mRNPs for remodeling by Dbp5[28], the Nup42 CTD ensures activation of Dbp5 (via the Gle1-Nup42 CTD interaction) when Mex67-bound mRNPs are present (via the Nup42 FG-Mex67 interaction). We propose that Nup42 serves as an important sensor that couples these steps in the mechanism. We anticipate that these interactions might direct specific interaction between Dbp5/DDX19B and mRNA to enable remodeling of specific proteins. As other DEAD-box proteins are activated by interaction partners in a similar manner to Gle1 activation of Dbp5 (eIF4G for eIF4A and THO for Sub2[45,46]), similar mechanisms might exist to spatially regulate these activities. This work also illustrates how Nup42/hNup42 as a specific binding partner at the NPC cytoplasmic face allows specificity to Gle1 and hGle1B function differentially from cytoplasmic Gle1/hGle1A function. With *S. cerevisiae* Nup42 being specifically required for heat shock mRNA export, we propose that Nup42 binding might also preferentially stabilize Gle1 and confer thermostability on the mRNA export mechanism. As such, this might explain how the Nup42/Gle1-mediated mRNA export mechanism is crucial under heat shock conditions.

One important distinction between the Dbp5 and DDX19B activities might be linked to a role for potential post-translational modifications or small effectors in the human system. A recent study reported roles for DDX19B phosphorylation in altering its nuclear activity during the DNA damage response[40]. We show here that DDX19B* purified from bacteria is not activated by hgle1-CTD in the presence of IP_6 or hnup42-CTD, and demonstrates relatively low enzymatic activity (Figure S4). In contrast, DDX19B purified from insect cells shows full, conserved functionality, including gle1-CTD-mediated stimulation that is enhanced in the presence of hnup42-CTD or IP_6 (Figure 6). Our future studies will be

focused on pinpointing potential DDX19B modifications needed for activity and regulation during mRNA export.

To further delineate the mRNA export mechanism, additional structural details regarding hNup42 and hGle1B molecular interactions in the context of the NPC are needed, and further analysis is required to fully understand how the mRNP remodeling platform is arranged to interact with exporting mRNPs. Overall, we demonstrate that the NPC protein Nup42 interacts with Gle1/hGle1B to locally regulate Dbp5/DDX19B activity. Importantly, this work demonstrates a remarkable conservation of function for the mRNP remodeling factors Gle1/hGle1B, Nup42/hNup42, Dbp5/DDX19B, and IP_6 during mRNA export in human and *S. cerevisiae* cells. These results also reveal novel unexpected steps in the molecular mechanism for mRNA export at the NPC cytoplasmic face that impact normal and disease cell function.

METHODS

Yeast Strains, Growth, and Y2H Analysis

Table S1 lists the yeast strains used in this study. Yeast genetic methods including mating, sporulation, dissection, and transformations were conducted according to standard procedures[47]. Yeast strains were grown at indicated temperatures in either YPD (2% peptone, 2% dextrose, 1% yeast extract) or selective minimal media lacking appropriate amino acids and supplemented with 2% dextrose and 5-fluoroorotic acid (5-FOA; United States Biological) as needed at 1.0 mg/mL. For growth analysis on plates, indicated strains were grown in YPD liquid media to mid-log phase (OD_{600} ~0.5), serially diluted, and equal numbers of cells were spotted onto YPD media for growth at the indicated temperatures. For Y2H analysis, vectors expressing GBD and GAD fusions were transformed into the reporter strain (PJ69-4A) or *nup42Δ* reporter strain (SWY6432) and selected on –Trp –Leu synthetic media. The resulting strains were then grown to mid-log phase, serially diluted, and equal numbers of cells were spotted onto –Trp –Leu or –Trp –Leu –His –Ade media. The plates were then incubated at 23°C for the indicated number of days.

Vector Construction

Table S2 lists the vectors used in this study. Vectors were cloned using standard molecular biology strategies or by Gibson Assembly (New England Biolabs, Ipswich, MA), and site-directed mutagenesis was performed using QuikChange (Agilent Genomics, Santa Clara, CA), and sequencing confirmed all vectors generated.

Live Cell Microscopy

Yeast strains were grown to mid-log phase in YPD or synthetic media lacking appropriate amino acids at the indicated temperatures. Cultures were collected, re-suspended in synthetic complete media at room temperature, and imaged. Wide-field images were acquired using a microscope (BX50; Olympus) equipped with a motorized stage (Model 999000, Ludl), Olympus 100× NA1.3 UPlanF1 objective, and digital charge coupled device camera (Orca-R2; Hamamatsu). Images were processed with ImageJ (NIH) or Adobe Photoshop CS6.

Heat Shock Protein Production Assay

The [^{35}S]methionine incorporation assay of heat shock proteins was performed as described[28,48]. Nascently produced radiolabeled proteins from whole-cell lysate were separated by SDS-PAGE, and the resulting gel was dried and exposed to autoradiography film.

Immunoblotting

For immunoblotting of yeast *S. cerevisiae* whole-cell lysates, cells were cultured and lysates were prepared as previously described in SDS loading buffer[28]. Proteins were resolved by SDS-PAGE and blotted using affinity-purified guinea pig anti-Gle1 (ASW 43[10]), rabbit anti-GFP (Thermo Fisher Scientific, Waltham, MA), or anti-yPgk1 (Thermo Fisher Scientific). IRDye 800CW-conjugated goat anti-mouse (LI-COR, Lincoln, NE) or Alexa Fluor 700 goat anti-rabbit (Thermo Fisher Scientific) antibodies (1:5000) were visualized with the Li-Cor Odyssey scanner (Lincoln, NE).

For HeLa cell lysate immunoblotting, cells were grown in 60 mm dishes (Fisher Scientific, Pittsburg, PA) and lysed in RIPA buffer (Sigma, St. Louis, MO) supplemented with EDTA-free cOmplete protease inhibitor cocktail (Roche Applied Science, Indianapolis, IN). Proteins were resolved by SDS-PAGE and blotted with rat anti-mCherry (Sigma), anti-hNup42/NUPL2 (Sigma), mouse anti-beta-actin (Sigma), or anti-hGle1[17] antibodies. Infrared 700- or 800-conjugated secondary antibodies (Thermo Fisher Scientific) were visualized with the Li-Cor Odyssey scanner.

HeLa cell culture and transfection

HeLa cells were cultured in complete DMEM media (Thermo Fisher Scientific) supplemented with 10% fetal bovine serum (FBS, Atlanta Biologicals, Norcross, GA) at 37°C in 5% CO_2. Knockdown add-back of *hGLE1* was performed using the previously validated protocol[17]. Negative control siRNA and *hGLE1* siRNAs were purchased from Qiagen (Valencia, CA). *hNUP42* SMARTpool siRNA was purchased from Dharmacon (Lafayette, CO). Cells were reverse-transfected with indicated 25 nM siRNAs using HiPerFect (Qiagen) and then transfected 24 h later with relevant constructs (siRNA-resistant *mCherry-hGLE1B^{R}* or *mCherry-hgle1B$^{R\text{-}QKED>AAAA}$* for Figure 4; siRNA-resistant *GFP-hGLE1B^{R}* or *GFP-hgle1B$^{R\text{-}KK>QQ}$* for Figure 5) using Fugene 6 (Promega, Madison, WI) per manufacturer's instructions.

HeLa immunofluorescence

HeLa cells expressing *mCherry-hGLE1B^{R}* and *mCherry-hgle1B$^{R\text{-}QKED>AAAA}$* were grown on 1.5 mm round coverslips in a 24-well plate (Fisher Scientific) and immunofluorescence was performed as previously described[18] using mAb414 (Biolegend, San Diego, CA) and anti-mCherry (Sigma). Cells were imaged using a 63x/1.4 NA oil-immersion objective on a confocal microscope (Leica TCS Sp5). Images were processed with ImageJ (NIH) or Adobe Photoshop CS6.

HeLa mRNA export assay

The previously validated knockdown add back approach (for *hGLE1*[17] or described *hNUP42* knockdown was employed followed by *in situ* hybridization of 488-oligo d(T) to poly(A)$^+$ RNA. Cells were imaged using a 63x/1.4 NA oil-immersion objective on a confocal microscope (Leica TCS Sp5). The nuclear:cytoplasmic ratio was determined by measuring mean intensity of these compartments in Image J (NIH) and dividing nuclear by cytoplasmic signal. Images were processed with ImageJ (NIH) or Adobe Photoshop CS6.

Protein Expression and Purification

Proteins were expressed (except DDX19B* and H_6-DDX19B) in *E. coli* Rosetta cells (Novagen) cultured in Terrific Broth under chloramphenicol and corresponding plasmid antibiotic resistance (kanamycin or ampicillin) selection. Protein expression was induced with IPTG (0.2 mM) at an OD_{600} of 0.5–0.8 for 18 hours at 18°C. Bacteria were lysed by sonication in Buffer B (20 mM HEPES (pH 7.5), 150 mM NaCl, 0.5 mM DTT, and 20% glycerol) supplemented with EDTA-free cOmplete protease inhibitor cocktail (Sigma) and 2 mM PMSF. All purified proteins were snap-frozen in an ethanol-dry ice bath and stored at −80°C.

The H_6-DDX19B plasmid was transformed into DH10Bac™ (Thermo Fisher Scientific) *E. coli* cells and plated on Luria agar plates containing tetracycline (10 μg/mL), gentamycin (7 μg/mL), kanamycin (50 μg/mL), IPTG (40 μg/mL), and X-Gal (100 μg/mL). White colonies were re-struck three times before the recombinant bacmid was purified from 1.5 mL of an overnight culture in LB containing tetracycline, gentamycin, and kanamycin. Transposition was verified by PCR with M13/pUC forward and reverse sequencing primers. Sf9 cells were cultured in Sf-900(TM) III SFM (Thermo Fisher Scientific) at 27°C. P0 virus stocks were generated by transfecting Sf9 cells (2 mL at 0.5×10^6 cells/mL) in a 6-well plate using Cellfectin(R) II Reagent (Thermo Fisher Scientific) and harvested three days post transfection. P1 virus was generated by adding 0.25 mL of P0 stock to 100-mm Petri dishes containing 10 mL of cells at 1×10^6 cells/mL and harvested three days post infection. P2 virus stocks were generated by adding 0.2 mL of P1 virus stocks to 20 mL of 1×10^6 cells/mL Sf9 cells in 125 mL shake flasks. P2 virus stocks were harvested after three days post infection with shaking at 140 rpm. Protein expression was achieved using High Five™ cells (Thermo Fisher Scientific), which were cultured in Express Five(R) SFM (Thermo Fisher Scientific) at 27°C with shaking at 140 rpm. P2 virus stocks (10 mL) were used to infect 450 mL of High Five™ cells (1×10^6 cells/mL) in 1 L shake flasks. High Five™ cells were harvested 48 hrs post infection and lysed using a Dounce homogenizer in the presence of Buffer B and 2 mM PMSF.

For MBP, MBP-gle1-CTD^{H337R}, H_6-MBP-TEV-gle1-CTD, H_6-MBP-TEV-gle1-CTD$^{QKEE>AAAA}$, H_6-MBP-TEV-hgle1B-CTD, H_6-MBP-PPS-hgle1B-CTD$^{QKED>AAAA}$, H_6-MBP-PPS-hgle1B-CTD$^{KK>QQ}$, and H_6-MBP-PPS-hgle1B-CTD$^{KKKK>QQQQ}$ proteins, the soluble fractions were purified with amylose resin (New England Biolabs) according to manufacturer recommendations. The amino-terminal tags on H_6-MBP-TEV-gle1-CTD, H_6-MBP-TEV-gle1-CTD$^{QKEE>AAAA}$, H_6-MBP-TEV-hgle1B-CTD, H_6-MBP-PPS-hgle1B-CTD$^{QKED>AAAA}$, H_6-MBP-PPS-hgle1B-CTD$^{KK>QQ}$, and H_6-MBP-PPS-hgle1B-

$CTD^{KKKK>QQQQ}$ were cleaved by addition of H_6-TEV or H_6-PPS to the amylose elution fractions and incubation overnight at 4°C. His-MBP and protease were removed by collecting flow-through after Ni Immobilized Metal Affinity Chromatography (Ni IMAC) (New England Biolabs). Flow-through was dialyzed overnight in Buffer B.

H_6-DDX19B and H_6-nup42-CTD were purified by Ni IMAC. Elution fractions were pooled and dialyzed overnight in Buffer B (H_6-nup42-CTD) or Buffer B with 400 mM NaCl (H_6-DDX19B).

GST, GST-Dbp5, GST-$dbp5^{L327V}$, GST-nup42-CTD, and GST-hnup42-CTD were purified by glutathione-coupled Sepharose chromatography. For GST-Dbp5, GST-$dbp5^{L327V}$, and GST-hnup42-CTD, the GST tag was cleaved by Factor Xa (New England Biolabs) digestion and inactivated by the addition of PMSF. The GST tag was removed from $dbp5^{L327V}$ by ion-exchange chromatography as in[4]. All proteins were dialyzed overnight in Buffer B.

GST-DDX19B* was expressed in *E. coli* Rosetta cells cultured in Terrific Broth under ampicillin and chloramphenicol antibiotic selection. Protein expression was induced with IPTG (0.1 mM) at an OD_{600} of 0.8 at 18°C for 18 hours. The harvested cell pellet was suspended in 30 mM HEPES pH 7.5, 400 mM NaCl, 10% Glycerol, 1 mM DTT, 2 mM $MgCl_2$ supplemented with ETDA-free cOmplete protease inhibitor cocktail and 2 mM PMSF and cells were lysed by sonication. Cleared lysate was incubated with buffer equilibrated glutathione-coupled sepharose 4B resin for 1.5 hours at 4°C with rotation. The resin was washed with 12 column volumes of buffer before elution with 10 mM reduced glutathione. The GST tag was removed by Factor Xa incubation for 36 hours at 4°C after the NaCl concentration was reduced to 200 mM by dilution with buffer containing no NaCl. GST was removed by passing the protein over buffer-equilibrated glutathione-coupled sepharose 4B resin and collecting the flow through. Protein homogeneity was verified by SDS-PAGE.

ATPase Assay

Colorimetric enzyme-coupled ATPase rate assays were performed as described[5]. Briefly, reaction mixtures (100μL), containing 10 mM HEPES (pH 7.5), 45 mM NaCl, 2 mM $MgCl_2$, 1 mM DTT, 20U SUPERase·In™ RNase Inhibitior (Thermo Fisher Scientific), 6 mM PEP (Sigma), 1.2 mM NADH (Sigma), 2.5 mM ATP (Sigma), 2 μL PK/LDH (Sigma), 1 μM polyA RNA, 500 nM Dbp5 or H_6-DDX19B, 1 μM IP_6 (Sigma, as indicated), 250 nM gle1-CTD or hgle1B-CTD (or mutants), and titration of H_6-nup42-CTD or hnup42-CTD as indicated. A_{340} was monitored every 40 sec for 40 min at 37°C in a BioTek Synergy HT microplate reader. Kcat/sec was calculated as $(((OD_{340}/\text{min} \times 2.5)/6.22\times10^{-3})/\mu\text{M protein})$.

BioLayer Interferometry

BioLayer interferometry assays were performed utilizing a ForteBIO Octet-Red96 at the Vanderbilt Antibody and Protein Resource Core. Biotinylated $nup42^{408–424}$ peptide (GenScript, Piscataway, NJ) was immobilized on a streptavidin conjugated biosensor at a well concentration of 0.5 μM in buffer containing 20 mM HEPES (pH 7.4), 200 mM NaCl, 1 mM DTT, 10% glycerol, 0.25 mM IP_6, and 0.01% Nonidet P-40. Immobilization was carried out over 5 minutes, followed by a 5-minute incubation in 100 μg/mL biocytin to cap

any free streptavidin sites on the biosensor surface. Following a 5-minute wash and 1-minute baseline, gle1-CTD or gle1-CTD$^{QKEE>AAAA}$ was allowed to associate for 5 minutes. Dissociation was followed for an addition 5 minutes. A single biosensor was used to measure binding at each concentration in parallel and responses in buffer alone were used to control for signal drift. The data analysis software provided by ForteBio was used to normalize all responses to an appropriate baseline, and subtract the buffer only control. The K_D was calculated from the determined k_{on} and k_{off} rates for the interaction.

In vitro binding assay

400 pmol GST or GST-nup42-CTD, 250 pmol MBP or MBP-gle1^{H337R}-CTD, and 500 pmol dbp5^{L327V} were incubated with equilibrated glutathione-coupled Sepharose in Buffer B. IP_6, ADP, or AMP-PNP, were added at 50 μM. Samples were incubated at 4°C for 2 hours and washed three times with Buffer B (IP_6, ADP, or AMP-PNP added in wash buffer where appropriate). Bound proteins were eluted in SDS loading buffer, resolved on a 12% (bottom) 7.5% (top) Tris-Glycine gel, and Coomassie stained.

Supplementary Material

Refer to Web version on PubMed Central for supplementary material.

Acknowledgments

The authors thank the Wente laboratory, particularly Renee Dawson, PhD, for discussions and critical reading of the manuscript; Andre Hoelz, PhD, (California Institute of Technology) for communicating results prior to publication; Rob Carnahan, PhD and Matt Goff (Vanderbilt Antibody and Protein Resource) for BioLayer Interferometry assistance; the Vanderbilt Central for Structural Biology for pSV282; Françoise Stutz, PhD, (Geneva) for pFS507; Brandt Eichman, PhD, (Vanderbilt) for use of equipment in purification from insect cells. This work was supported by grants from the National Institutes of Health (R37GM051219 [S.R.W.] and training position on T32HD007502 [R.L.A.]).

References

1. Fernandez-Martinez J, Kim SJ, Shi Y, et al. Structure and Function of the Nuclear Pore Complex Cytoplasmic mRNA Export Platform. Cell. 2016; 167(5):1215–1228.e25. DOI: 10.1016/j.cell.2016.10.028 [PubMed: 27839866]
2. Oeffinger M, Zenklusen D. To the pore and through the pore: a story of mRNA export kinetics. Biochim Biophys Acta. 2012; 1819(6):494–506. DOI: 10.1016/j.bbagrm.2012.02.011 [PubMed: 22387213]
3. Lund MK, Guthrie C. The DEAD-box protein Dbp5p is required to dissociate Mex67p from exported mRNPs at the nuclear rim. Mol Cell. 2005; 20(4):645–651. DOI: 10.1016/j.molcel.2005.10.005 [PubMed: 16307927]
4. Tran EJ, Zhou Y, Corbett AH, Wente SR. The DEAD-box protein Dbp5 controls mRNA export by triggering specific RNA:protein remodeling events. Mol Cell. 2007; 28(5):850–859. DOI: 10.1016/j.molcel.2007.09.019 [PubMed: 18082609]
5. Noble KN, Tran EJ, Alcázar-Román AR, Hodge CA, Cole CN, Wente SR. The Dbp5 cycle at the nuclear pore complex during mRNA export II: nucleotide cycling and mRNP remodeling by Dbp5 are controlled by Nup159 and Gle1. Genes Dev. 2011; 25(10):1065–1077. DOI: 10.1101/gad.2040611 [PubMed: 21576266]
6. Alcázar-Román AR, Tran EJ, Guo S, Wente SR. Inositol hexakisphosphate and Gle1 activate the DEAD-box protein Dbp5 for nuclear mRNA export. Nat Cell Biol. 2006; 8(7):711–716. DOI: 10.1038/ncb1427 [PubMed: 16783363]

7. Montpetit B, Thomsen ND, Helmke KJ, Seeliger MA, Berger JM, Weis K. A conserved mechanism of DEAD-box ATPase activation by nucleoporins and InsP6 in mRNA export. Nature. 2011; 472(7342):238–242. DOI: 10.1038/nature09862 [PubMed: 21441902]
8. Weirich CS, Erzberger JP, Flick JS, Berger JM, Thorner J, Weis K. Activation of the DExD/H-box protein Dbp5 by the nuclear-pore protein Gle1 and its coactivator InsP6 is required for mRNA export. Nat Cell Biol. 2006; 8(7):668–676. DOI: 10.1038/ncb1424 [PubMed: 16783364]
9. Murphy R, Wente SR. An RNA-export mediator with an essential nuclear export signal. Nature. 1996; 383(6598):357–360. DOI: 10.1038/383357a0 [PubMed: 8848052]
10. Alcázar-Román AR, Bolger TA, Wente SR. Control of mRNA export and translation termination by inositol hexakisphosphate requires specific interaction with Gle1. J Biol Chem. 2010; 285(22): 16683–16692. DOI: 10.1074/jbc.M109.082370 [PubMed: 20371601]
11. Watkins JL, Murphy R, Emtage JL, Wente SR. The human homologue of Saccharomyces cerevisiae Gle1p is required for poly(A)+ RNA export. Proc Natl Acad Sci U S A. 1998; 95(12): 6779–6784. [PubMed: 9618489]
12. Bolger TA, Wente SR. Gle1 is a multifunctional DEAD-box protein regulator that modulates Ded1 in translation initiation. J Biol Chem. 2011; 286(46):39750–39759. DOI: 10.1074/jbc.M111.299321 [PubMed: 21949122]
13. Bolger TA, Folkmann AW, Tran EJ, Wente SR. The mRNA export factor Gle1 and inositol hexakisphosphate regulate distinct stages of translation. Cell. 2008; 134(4):624–633. DOI: 10.1016/j.cell.2008.06.027 [PubMed: 18724935]
14. Gross T, Siepmann A, Sturm D, et al. The DEAD-box RNA helicase Dbp5 functions in translation termination. Science. 2007; 315(5812):646–649. DOI: 10.1126/science.1134641 [PubMed: 17272721]
15. Aryanpur PP, Regan CA, Collins JM, et al. Gle1 regulates RNA binding of the DEAD-box helicase Ded1 in its complex role in translation initiation. Mol Cell Biol. Aug.2017 doi: 10.1128/MCB.00139-17
16. Kendirgi F, Barry DM, Griffis ER, Powers MA, Wente SR. An essential role for hGle1 nucleocytoplasmic shuttling in mRNA export. J Cell Biol. 2003; 160(7):1029–1040. DOI: 10.1083/jcb.200211081 [PubMed: 12668658]
17. Folkmann AW, Collier SE, Zhan X, Aditi, Ohi MD, Wente SR. Gle1 functions during mRNA export in an oligomeric complex that is altered in human disease. Cell. 2013; 155(3):582–593. DOI: 10.1016/j.cell.2013.09.023 [PubMed: 24243016]
18. Aditi, Folkmann AW, Wente SR. Cytoplasmic hGle1A regulates stress granules by modulation of translation. Mol Biol Cell. 2015; 26(8):1476–1490. DOI: 10.1091/mbc.E14-11-1523 [PubMed: 25694449]
19. Jao L-E, Akef A, Wente SR. A role for Gle1, a regulator of DEAD-box RNA helicases, at centrosomes and basal bodies. Mol Biol Cell. 2017; 28(1):120–127. DOI: 10.1091/mbc.E16-09-0675 [PubMed: 28035044]
20. Folkmann AW, Noble KN, Cole CN, Wente SR. Dbp5, Gle1-IP6 and Nup159: a working model for mRNP export. Nucl Austin Tex. 2011; 2(6):540–548. DOI: 10.4161/nucl.2.6.17881
21. Rayala HJ, Kendirgi F, Barry DM, Majerus PW, Wente SR. The mRNA export factor human Gle1 interacts with the nuclear pore complex protein Nup155. Mol Cell Proteomics MCP. 2004; 3(2): 145–155. DOI: 10.1074/mcp.M300106-MCP200 [PubMed: 14645504]
22. Kendirgi F, Rexer DJ, Alcázar-Román AR, Onishko HM, Wente SR. Interaction between the shuttling mRNA export factor Gle1 and the nucleoporin hCG1: a conserved mechanism in the export of Hsp70 mRNA. Mol Biol Cell. 2005; 16(9):4304–4315. DOI: 10.1091/mbc.E04-11-0998 [PubMed: 16000379]
23. Strahm Y, Fahrenkrog B, Zenklusen D, et al. The RNA export factor Gle1p is located on the cytoplasmic fibrils of the NPC and physically interacts with the FG-nucleoporin Rip1p, the DEAD-box protein Rat8p/Dbp5p and a new protein Ymr 255p. EMBO J. 1999; 18(20):5761–5777. DOI: 10.1093/emboj/18.20.5761 [PubMed: 10610322]
24. Jao L-E, Appel B, Wente SR. A zebrafish model of lethal congenital contracture syndrome 1 reveals Gle1 function in spinal neural precursor survival and motor axon arborization. Dev Camb Engl. 2012; 139(7):1316–1326. DOI: 10.1242/dev.074344

25. Nousiainen HO, Kestilä M, Pakkasjärvi N, et al. Mutations in mRNA export mediator GLE1 result in a fetal motoneuron disease. Nat Genet. 2008; 40(2):155–157. DOI: 10.1038/ng.2007.65 [PubMed: 18204449]
26. Aditi, Glass L, Dawson TR, Wente SR. An amyotrophic lateral sclerosis-linked mutation in GLE1 alters the cellular pool of human Gle1 functional isoforms. Adv Biol Regul. 2016; 62:25–36. DOI: 10.1016/j.jbior.2015.11.001 [PubMed: 26776475]
27. Kaneb HM, Folkmann AW, Belzil VV, et al. Deleterious mutations in the essential mRNA metabolism factor, hGle1, in amyotrophic lateral sclerosis. Hum Mol Genet. 2015; 24(5):1363–1373. DOI: 10.1093/hmg/ddu545 [PubMed: 25343993]
28. Adams RL, Terry LJ, Wente SR. Nucleoporin FG domains facilitate mRNP remodeling at the cytoplasmic face of the nuclear pore complex. Genetics. 2014; 197(4):1213–1224. DOI: 10.1534/genetics.114.164012 [PubMed: 24931410]
29. Strässer K, Bassler J, Hurt E. Binding of the Mex67p/Mtr2p heterodimer to FXFG, GLFG, and FG repeat nucleoporins is essential for nuclear mRNA export. J Cell Biol. 2000; 150(4):695–706. [PubMed: 10952996]
30. Saavedra CA, Hammell CM, Heath CV, Cole CN. Yeast heat shock mRNAs are exported through a distinct pathway defined by Rip1p. Genes Dev. 1997; 11(21):2845–2856. [PubMed: 9353254]
31. Miller AL, Suntharalingam M, Johnson SL, Audhya A, Emr SD, Wente SR. Cytoplasmic inositol hexakisphosphate production is sufficient for mediating the Gle1-mRNA export pathway. J Biol Chem. 2004; 279(49):51022–51032. DOI: 10.1074/jbc.M409394200 [PubMed: 15459192]
32. Stutz F, Kantor J, Zhang D, McCarthy T, Neville M, Rosbash M. The yeast nucleoporin rip1p contributes to multiple export pathways with no essential role for its FG-repeat region. Genes Dev. 1997; 11(21):2857–2868. [PubMed: 9353255]
33. Rollenhagen C, Hodge CA, Cole CN. The Nuclear Pore Complex and the DEAD Box Protein Rat8p/Dbp5p Have Nonessential Features Which Appear To Facilitate mRNA Export following Heat Shock. Mol Cell Biol. 2004; 24(11):4869–4879. DOI: 10.1128/MCB.24.11.4869-4879.2004 [PubMed: 15143180]
34. Stutz F, Neville M, Rosbash M. Identification of a novel nuclear pore-associated protein as a functional target of the HIV-1 Rev protein in yeast. Cell. 1995; 82(3):495–506. [PubMed: 7634338]
35. Sievers F, Higgins DG. Clustal Omega, accurate alignment of very large numbers of sequences. Methods Mol Biol Clifton NJ. 2014; 1079:105–116. DOI: 10.1007/978-1-62703-646-7_6
36. Saavedra C, Tung KS, Amberg DC, Hopper AK, Cole CN. Regulation of mRNA export in response to stress in Saccharomyces cerevisiae. Genes Dev. 1996; 10(13):1608–1620. [PubMed: 8682292]
37. Slabinski L, Jaroszewski L, Rychlewski L, Wilson IA, Lesley SA, Godzik A. XtalPred: a web server for prediction of protein crystallizability. Bioinforma Oxf Engl. 2007; 23(24):3403–3405. DOI: 10.1093/bioinformatics/btm477
38. Hodge CA, Tran EJ, Noble KN, et al. The Dbp5 cycle at the nuclear pore complex during mRNA export I: dbp5 mutants with defects in RNA binding and ATP hydrolysis define key steps for Nup159 and Gle1. Genes Dev. 2011; 25(10):1052–1064. DOI: 10.1101/gad.2041611 [PubMed: 21576265]
39. Wickramasinghe VO, Savill JM, Chavali S, et al. Human inositol polyphosphate multikinase regulates transcript-selective nuclear mRNA export to preserve genome integrity. Mol Cell. 2013; 51(6):737–750. DOI: 10.1016/j.molcel.2013.08.031 [PubMed: 24074953]
40. Hodroj D, Recolin B, Serhal K, et al. An ATR-dependent function for the Ddx19 RNA helicase in nuclear R-loop metabolism. EMBO J. Mar.2017 doi: 10.15252/embj.201695131
41. Rajakylä EK, Viita T, Kyheröinen S, Huet G, Treisman R, Vartiainen MK. RNA export factor Ddx19 is required for nuclear import of the SRF coactivator MKL1. Nat Commun. 2015; 6:5978.doi: 10.1038/ncomms6978 [PubMed: 25585691]
42. Terry LJ, Wente SR. Nuclear mRNA export requires specific FG nucleoporins for translocation through the nuclear pore complex. J Cell Biol. 2007; 178(7):1121–1132. DOI: 10.1083/jcb.200704174 [PubMed: 17875746]

43. Hurwitz ME, Strambio-de-Castillia C, Blobel G. Two yeast nuclear pore complex proteins involved in mRNA export form a cytoplasmically oriented subcomplex. Proc Natl Acad Sci U S A. 1998; 95(19):11241–11245. [PubMed: 9736720]

44. Lee H-S, Lee D-H, Cho HK, Kim SH, Auh JH, Pai H-S. InsP6-sensitive variants of the Gle1 mRNA export factor rescue growth and fertility defects of the ipk1 low-phytic-acid mutation in Arabidopsis. Plant Cell. 2015; 27(2):417–431. DOI: 10.1105/tpc.114.132134 [PubMed: 25670768]

45. Ren Y, Schmiege P, Blobel G. Structural and biochemical analyses of the DEAD-box ATPase Sub2 in association with THO or Yra1. eLife. 2017; 6doi: 10.7554/eLife.20070

46. Schütz P, Bumann M, Oberholzer AE, et al. Crystal structure of the yeast eIF4A-eIF4G complex: an RNA-helicase controlled by protein-protein interactions. Proc Natl Acad Sci U S A. 2008; 105(28):9564–9569. DOI: 10.1073/pnas.0800418105 [PubMed: 18606994]

47. Sherman, F., Fink, GR., Hicks, JB. Laboratory Course Manual for Methods in Yeast Genetics. Cold Spring Harbor Laboratory; 1986.

48. Carmody SR, Tran EJ, Apponi LH, Corbett AH, Wente SR. The mitogen-activated protein kinase Slt2 regulates nuclear retention of non-heat shock mRNAs during heat shock-induced stress. Mol Cell Biol. 2010; 30(21):5168–5179. DOI: 10.1128/MCB.00735-10 [PubMed: 20823268]

SYNOPSIS

Activation of the DEAD-box ATPase Dbp5 by Gle1-IP_6 is required for mRNA export through nuclear pore complexes (NPCs). In this paper, Adams, et al. demonstrate that a constituent of the NPC, Nup42, impacts the ATPase activity of Dbp5 through interaction with Gle1. This function, as well as IP_6-hGle1B interaction, is required for mRNA export in human cells and altered in human diseases. This work reveals how Gle1-Dbp5 activity is locally coordinated for function at the proper place and time.

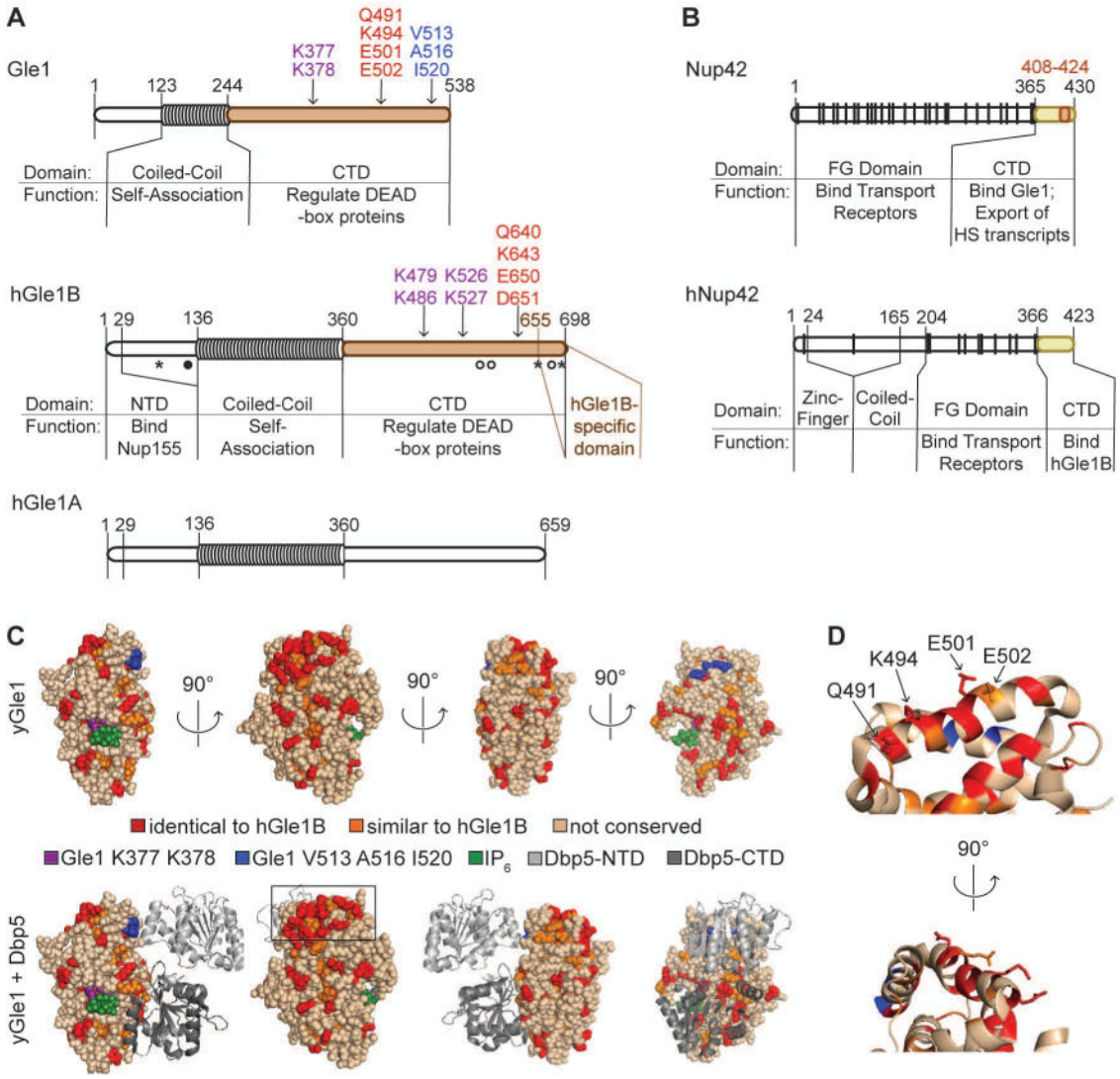

Figure 1. Gle1-Nup42 interaction domains

(A) Domain structure of Gle1, hGle1B, and hGle1A. For Gle1, K377 K378 indicates IP_6-coordinating residues identified in[10], V513 A516 I520 indicates residues essential for Dbp5 ATPase regulation[7], and Q491 K494 E501 E502 indicates residues essential for interaction with Nup42 identified in this paper. For hGle1B, K526 K527 are homologous to *S. cerevisiae* Gle1 K377 K378, with K479 K486 as additional positively-charged residues at the IP_6 interface (based on homologous residues in the Gle1 structure[7], PDB 3RRM), and Q640 K643 E650 D651 indicates residues essential for interaction with hNup42 identified in this paper. Symbols denote changes from disease-associated mutations[25,27]: asterisks are ALS-associated mutations, filled circle indicates LCCS1 Fin_{major}, open circles indicate other LCCS1 or LAAHD mutations. From amino to carboxy-terminus: S70X, ALS-associated nonsense mutation; T144_E145insPFQ, LCCS1 Fin_{major}; R569H, LCCS1; V617M, LAAHD; 654/IVS14-2A>C, ALS (alternate exon use results in novel C-terminal extension from this residue); I694T, LAAHD; R697C, ALS. (B) Domain structure of Nup42 and hNup42. For Nup42, 408–424 indicates minimal Gle1 interaction domain defined in this

paper. (A & B) Colored regions indicate truncations used in biochemistry experiments. (C) *S. cerevisiae* Gle1 contains a conserved patch of residues opposite the Dbp5 binding site. From a Clustal Omega[35] sequence alignment between Gle1 and hGle1B, identical (red) and similar (orange) residues were mapped onto the Gle1-Dbp5 structure[7], PDB 3RRM). (D) Q491, K494, E501, and E502 are surface accessible residues in the conserved patch on *S. cerevisiae* Gle1. Residues are indicated on zoomed region boxed in C.

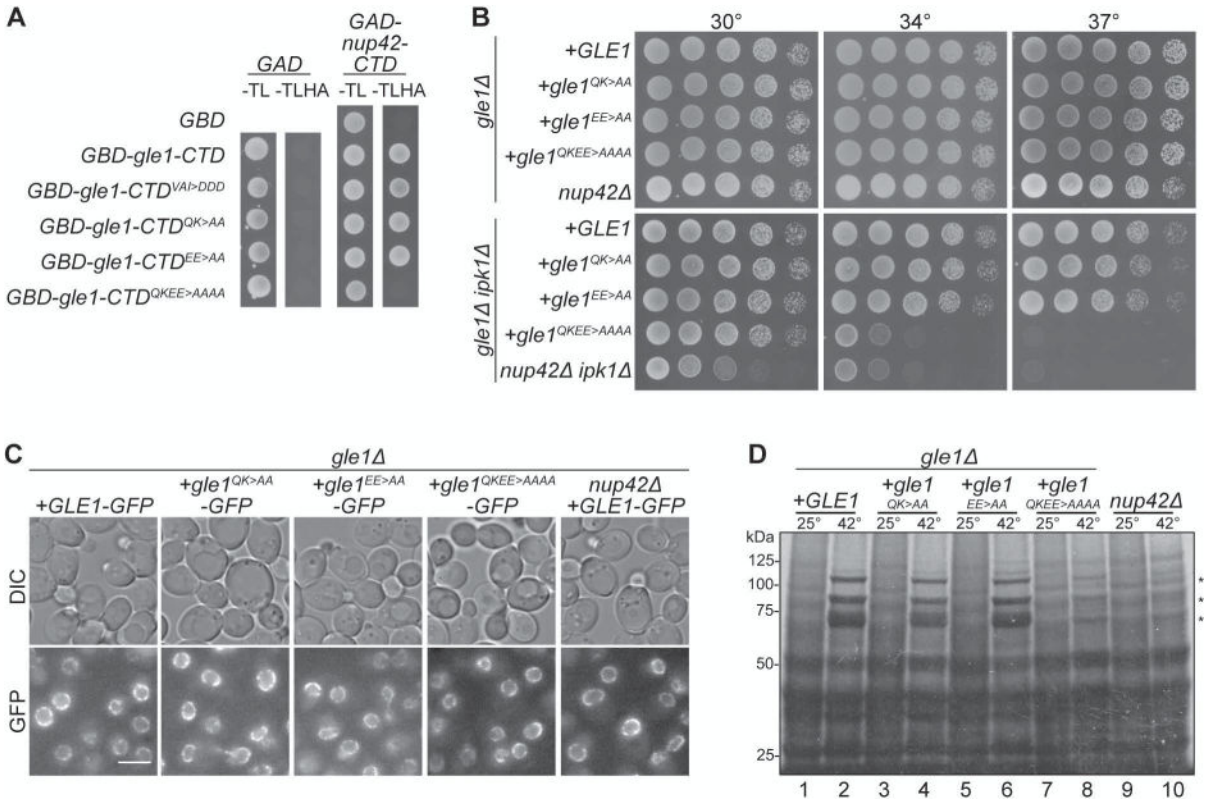

Figure 2. Functional analysis of the proposed Nup42 binding site on Gle1

(A) QKEE>AAAA disrupts the Gle1-Nup42 Y2H interaction. Indicated plasmids were transformed into the Y2H reporter strain, grown to early log phase at 23°C, and plated on the synthetic media lacking indicated amino acids for growth at 23°C. (B) *gle1*$^{QKEE>AAAA}$ *ipk1Δ* phenocopies the growth defect of *nup42Δ ipk1Δ*. Indicated strains were grown to mid-log phase, serially diluted, and plated on YPD for growth at the indicated temperatures. (C) Gle1 is localized at NPCs when interaction with Nup42 is disrupted. Indicated strains containing carboxy-terminal GFP-tagged *GLE1-GFP* plasmids were grown to mid-log phase in YPD at 23°C and live cells were imaged by wide-field microscopy. Scale bar = 5μm. (D) *gle1*$^{QKEE>AAAA}$ disrupts heat-shock mRNA export. Indicated strains were grown at 25°C to early-log phase, kept at 25°C or shifted to 42°C for 15 min, labeled with [^{35}S]methionine for an additional 15 min, and lysed. Lysates were separated by SDS-PAGE, and proteins were visualized by autoradiography. The positions of Hsp proteins, induced upon heat shock, are indicated by asterisks.

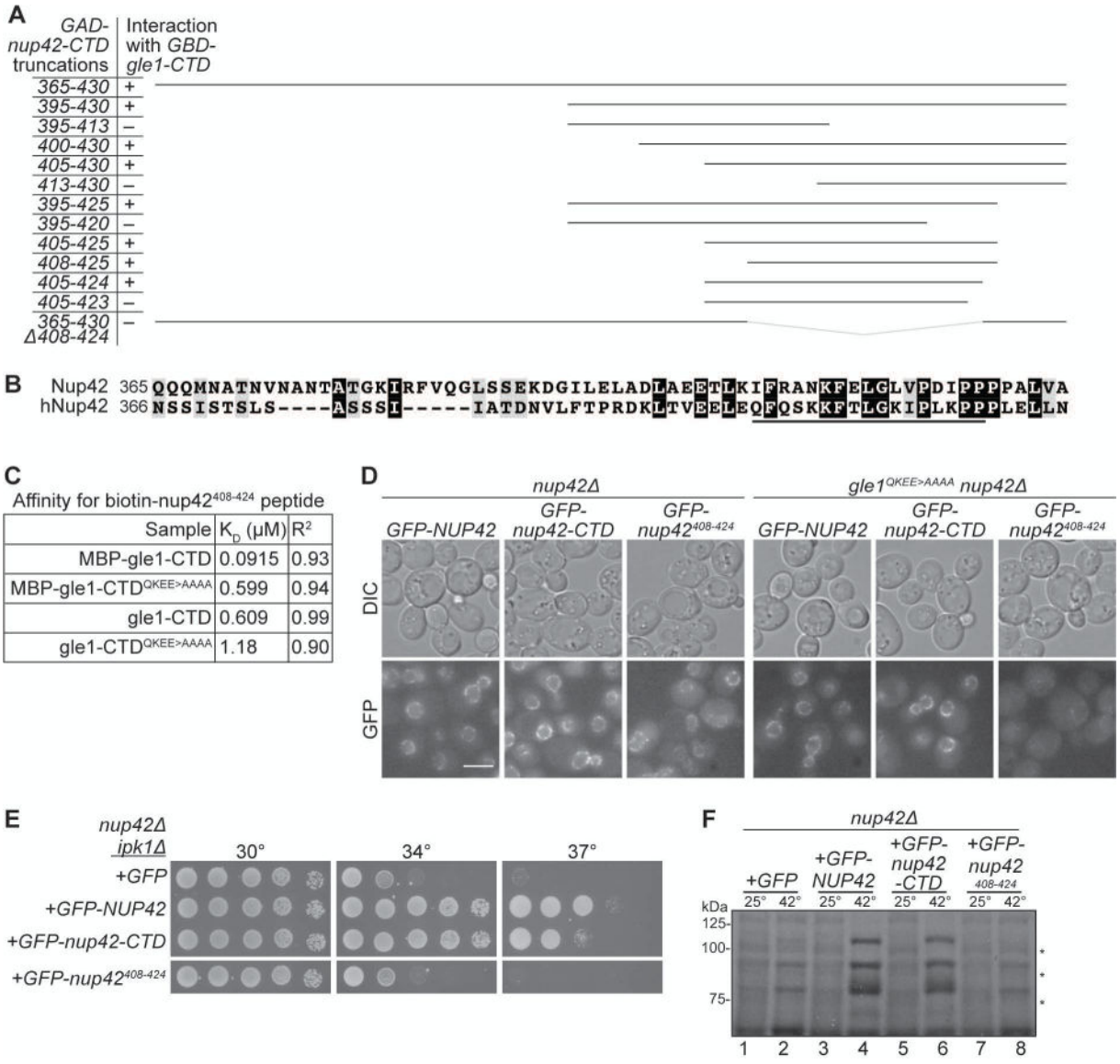

Figure 3. Analysis of minimal Gle1-binding domain in Nup42

(A) nup42$^{408–424}$ is required for interaction with Gle1. Indicated plasmids were transformed into the Y2H reporter strain, and struck to –Trp –Leu –His –Ade synthetic media for growth at 23°C. Growth on quadruple drop-out media is indicated as "+". (B) nup42$^{408–424}$ lies in a conserved region of the protein. Clustal Omega[35] alignment between nup42-CTD and hnup42-CTD. Identical (black) and similar (grey) residues are indicated. The black line above the sequence indicates residues 408–424 of Nup42. (C) Affinity measurements between gle1-CTD and nup42$^{408–424}$. BioLayer Interferometry was performed with a biotin-nup42$^{408–424}$ peptide and recombinant gle1-CTD protein. Calculated K_D and R^2 correlation is indicated. (D) GFP-nup42$^{408–424}$ localization at the nuclear envelope is disrupted in *gle1$^{QKEE>AAAA}$* mutants. Strains containing the indicated plasmids were grown to mid-log phase at 23°C and live cells were imaged by wide-field microscopy. Scale bar = 5μm. (E) *nup42$^{408–424}$* does not rescue the growth defect of *nup42Δ ipk1Δ* mutants. *nup42Δ ipk1Δ* was transformed with the indicated GFP-tagged constructs, grown to mid-log phase, and

plated on –Leu synthetic media for growth at the indicated temperatures. (F) *nup42*$^{408–424}$ is not sufficient for heat shock mRNA export. *nup42Δ* mutants were transformed with the indicated GFP-tagged constructs, grown at 25°C to early-log phase in synthetic media, kept at 25°C or shifted to 42°C for 15 min, labeled with [^{35}S]methionine for an additional 15 min, and lysed. Lysates were separated by SDS-PAGE, and proteins were visualized by autoradiography. Hsp proteins are indicated by asterisks.

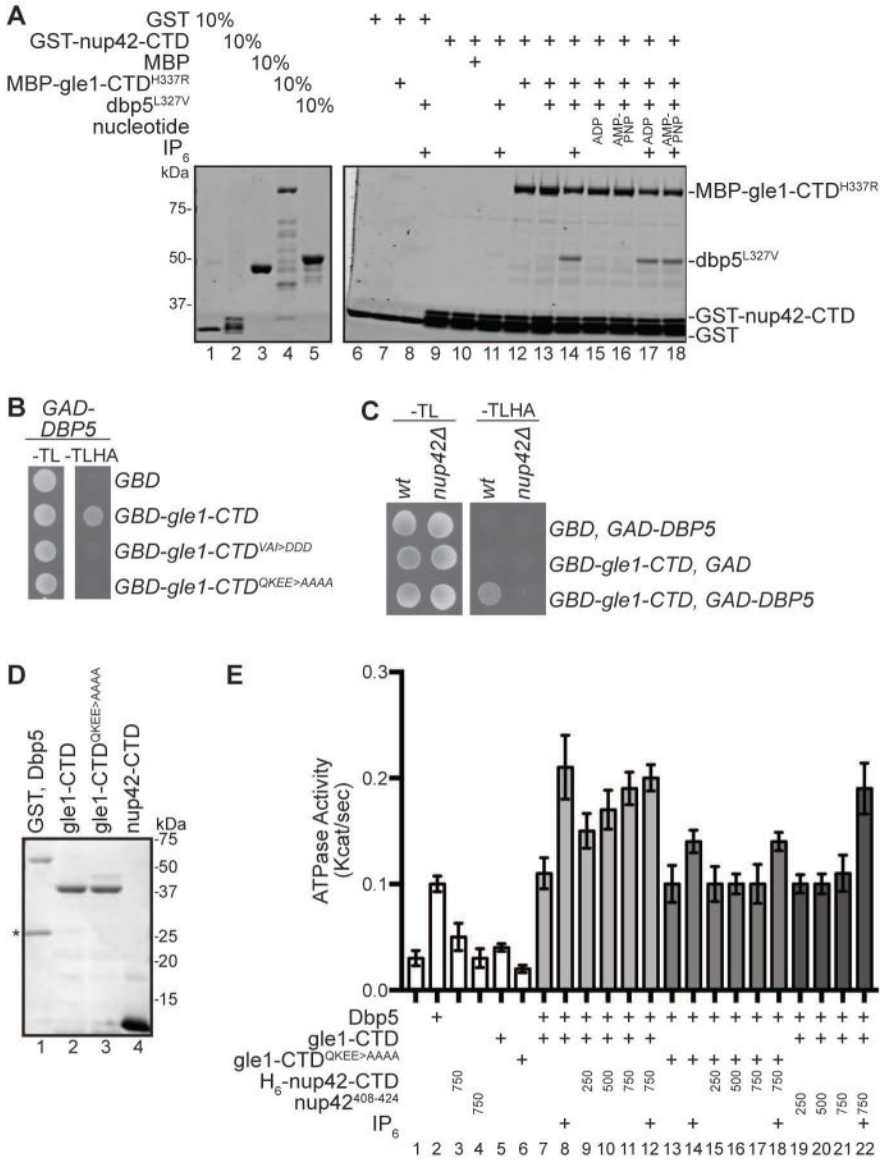

Figure 4. Nup42 coordinates Gle1-Dbp5 interaction

(A) Nup42, Gle1, and Dbp5 interact in a trimeric protein complex with IP_6. Soluble binding assays were conducted with purified recombinant proteins immobilized on glutathione coupled Sepharose. Input and bound fractions were analyzed by SDS-PAGE and Coomassie staining. Note: GST-nup42-CTD is proteolytically sensitive and resolves as several bands by SDS-PAGE (lane 2), as observed in[23]. (B) GBD-gle1-CTD$^{QKEE>AAAA}$ does not interact with GAD-Dbp5 via Y2H. Indicated plasmids were transformed into the Y2H reporter strain, grown to early log phase at 23°C, and plated on the synthetic media lacking indicated amino acids for growth at 23°C. (C) GBD-gle1-CTD does not interact with GAD-Dbp5 in *nup42Δ* mutants. Indicated plasmids were transformed into wild-type (wt) or *nup42Δ* Y2H reporter strains, grown to early log phase at 23°, and plated on the synthetic media lacking indicated amino acids for growth at 23°C. (D) Purified recombinant *S. cerevisiae* proteins used in ATPase assays. 1μg indicated proteins were resolved by SDS-PAGE and Coomassie

stained. Asterisk indicates GST cleaved (not removed) from Dbp5 sample. (E) nup42-CTD enhances Gle1 stimulation of Dbp5 ATPase activity in the absence of IP_6. PK/LDH-coupled ATPase assays were performed with Dbp5 (500 nM) in the presence of 1 μM A_{30} RNA and 2 mM ATP gle1-CTD or gle1-CTD$^{QKEE>AAAA}$ (250 nM), IP_6 (1 μM), and varying amounts of nup42-CTD or nup42$^{408–424}$ peptide (250, 500, or 750 nM) were added as indicated. Reactions were incubated at 37°C for 40 min with the A_{340} monitored every 40 seconds to calculate Kcat. Mean shown for n=3, and standard error is indicated by error bars.

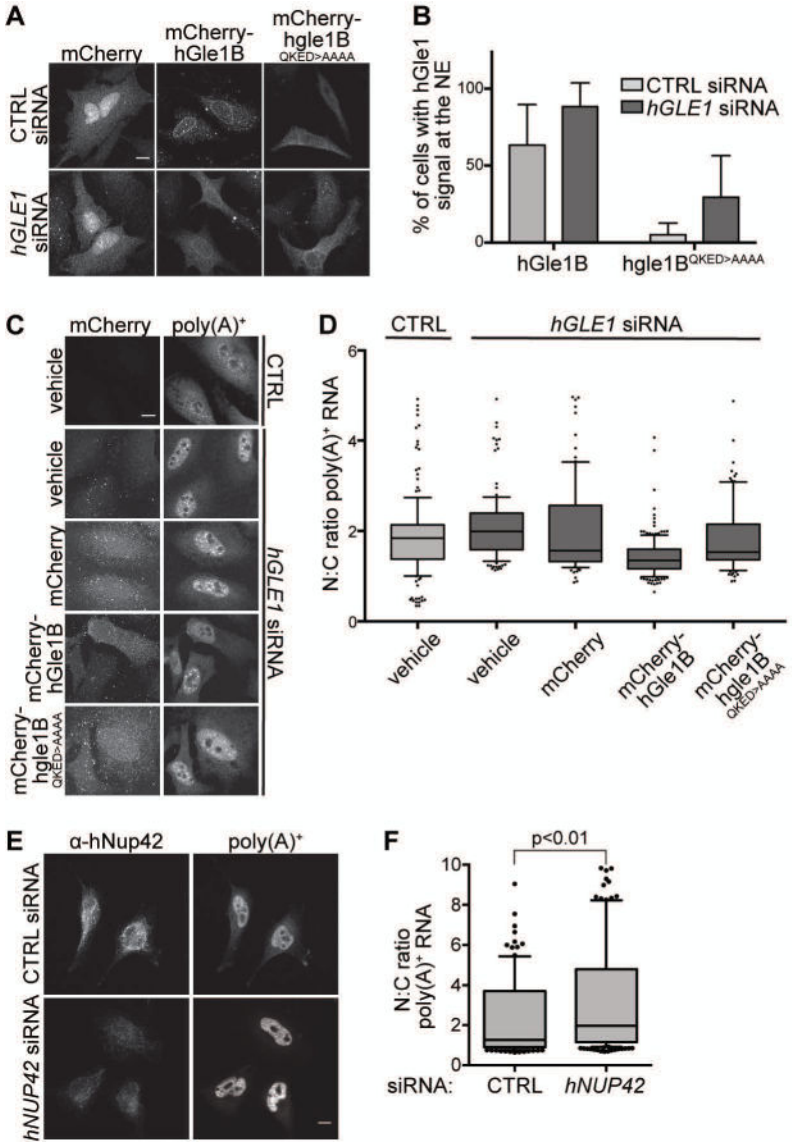

Figure 5. hGle1B interaction with hNup42 is required for mRNA export

(A–B) mCherry-hgle1B$^{QKED>AAAA}$ is localized to the nuclear rim in a portion of cells. (A) HeLa cells expressing exogenous siRNA-resistant *mCherry-hGLE1B^{R}* and *mCherry-hgle1B$^{R\text{-}QKED>AAAA}$* after treatment with CTRL or *hGLE1* siRNA were imaged by confocal microscopy. Scale bar=10μm. (B) Quantification of cells with rim-localized mCherry signal from the experiment in A. Approximately sixty cells were quantified from three independent experiments, and the mean is indicated with standard error indicated by error bars. (C-D) mCherry-hgle1B$^{QKED>AAAA}$ does not rescue the mRNA export defect upon *hGLE1* knockdown. (C) HeLa cells were transfected with *mCherry*, *mCherry-hGLE1B^{R}* or *mCherry-hgle1B$^{R\text{-}QKED>AAAA}$* plasmids following CTRL or *hGLE1* knockdown. After fixation, cells were processed for *in situ* hybridization using 488-labeled oligo d(T) probe followed by mCherry immunofluoresence. Scale bar=10μm. (D) Quantification of nuclear:cytoplasmic mean fluorescence intensity of oligo d(T) signal. Approximately 100 cells were quantified per condition from three independent experiments

with nuclear:cytoplasmic intensity ratio depicted in box and whisker plots (whiskers representing 10%–90%). Statistical analysis includes ANOVA with a post-hoc t-test. (E-F) *hNUP42* depletion results in a poly(A)$^+$ mRNA export defect. (E) HeLa cells were transfected with CTRL or *hNUP42* siRNA for 72h. After fixation, cells were processed for *in situ* hybridization using Cy3-labeled oligo d(T) probe followed by hNup42 immunofluorescence. Scale bar=10μm. (F) Quantification of nuclear:cytoplasmic mean fluorescence intensity of oligo d(T) signal. Approximately 200 cells were quantified per condition from three independent experiments with nuclear:cytoplasmic intensity ratio depicted in box and whisker plots (whiskers representing 10%–90%). A t-test was performed to analyze statistical significance.

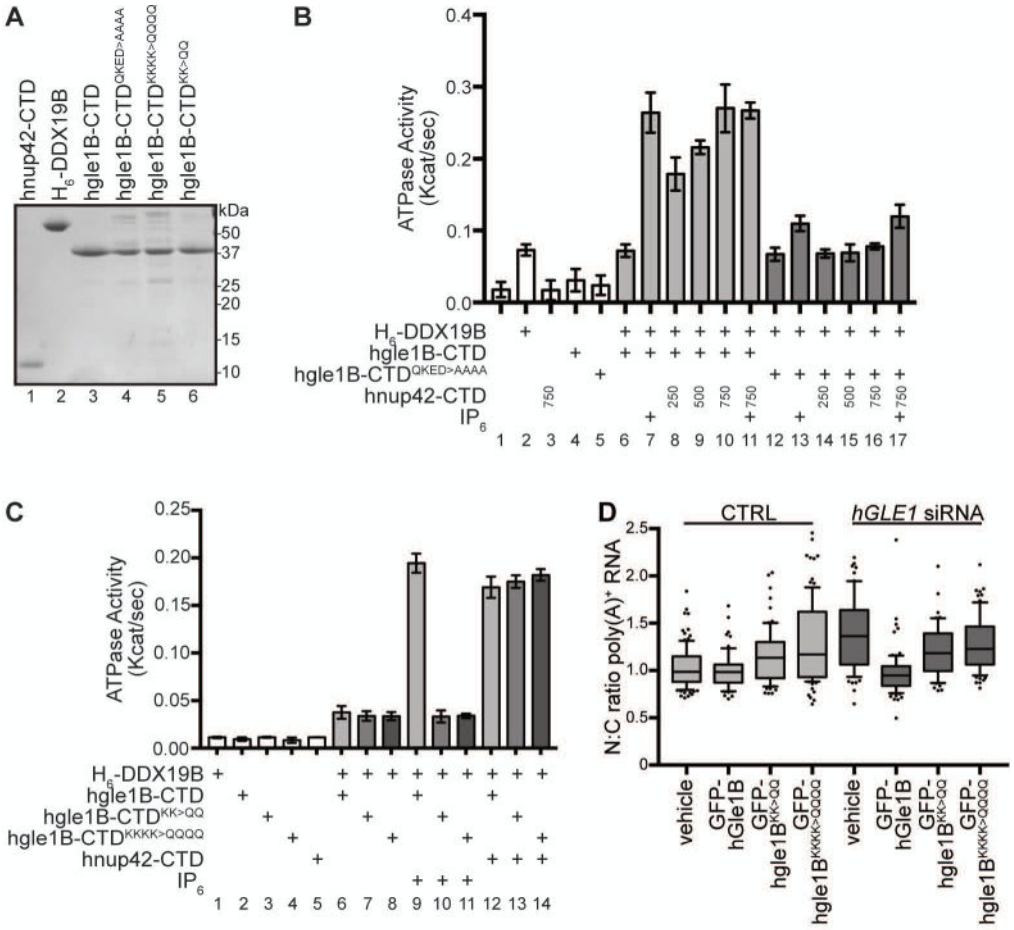

Figure 6. hGle1B interactions with hNup42 and IP_6 enhances stimulation of DDX19B activity and are required for mRNA export

(A) Purified recombinant human proteins used in ATPase assays. 1μg indicated purified proteins were resolved by SDS-PAGE and Coomassie stained. (B) hGle1B and hNup42 stimulate DDX19B ATPase activity in absence of IP_6. PK/LDH-coupled ATPase assays were performed with H_6-DDX19B (500 nM, expressed in insect cells) in the presence of 1 μM A_{30} RNA and 2 mM ATP. hgle1B-CTD or hgle1B-CTD$^{QKED>AAAA}$ (250 nM), IP_6 (1 μM), and varying amounts of hnup42-CTD (250, 500, or 750 nM) were added as indicated. Reactions preformed as in Figure 3D. Mean shown for n=3, and standard error is indicated by error bars. (C) hGle1B-IP_6 interaction is conserved in human proteins. PK/LDH-coupled ATPase assays were performed with H_6-DDX19B (500 nM) in the presence of 1 μM A_{30} RNA and 2 mM ATP, hgle1B-CTD, hgle1B-CTD$^{KK>QQ}$, or hgle1B-CTD$^{KKKK>QQQQ}$ (250 nM), and hnup42-CTD (750 nM) or IP_6 (1 μM) were added as indicated. Purified proteins are shown in 6A. Reactions performed as in Figure 3D. Mean shown for n=3, and standard error is indicated by error bars. (D) hGle1B-IP_6 interaction is required for mRNA export. HeLa cells were transfected with vehicle or *GFP-hGLE1B^{R}*, *GFP-hgle1B$^{R\text{-}KK>QQ}$*, or *GFP-hgle1B$^{R\text{-}KKKK>QQQQ}$* plasmids following CTRL or *hGLE1* knockdown. Nuclear:cytoplasmic mean fluorescence intensity of oligo d(T) signal was quantified as in Figure 5F.

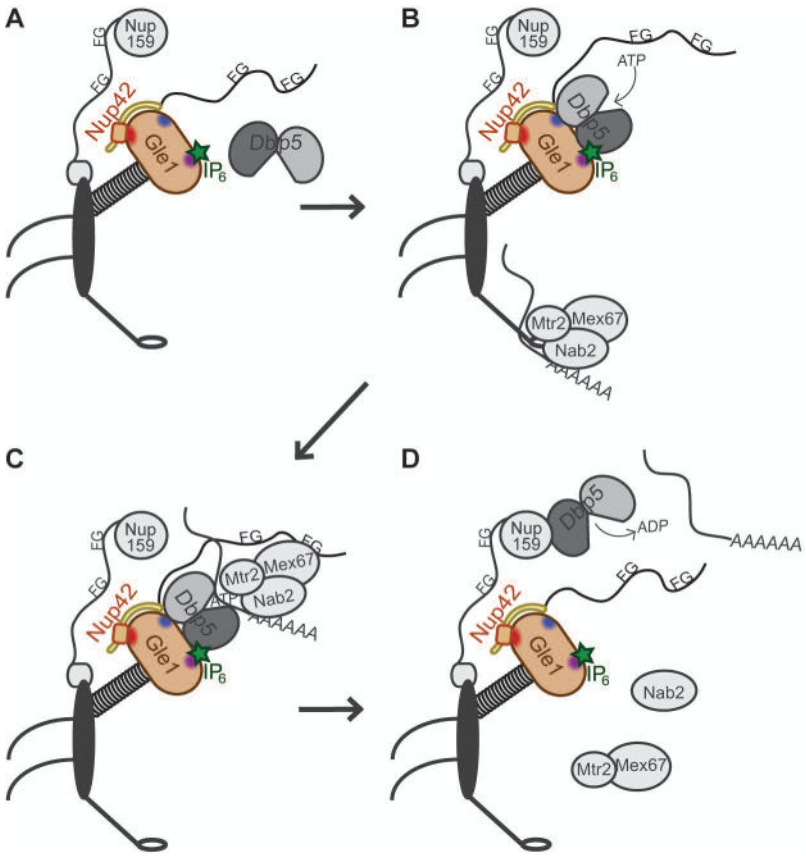

Figure 7. Schematic for Nup42 function at the NPC cytoplasmic face

(A) Dbp5 dynamically associates with the NPC. (B) The Nup42 CTD stimulates Gle1-IP_6 interaction with Dbp5, with Gle1-IP_6 promoting ATP loading onto Dbp5. Mature mRNPs interact with the Mex67-Mtr2 heterodimer via adaptors such as the poly(A)$^+$ binding protein Nab2, permitting export through the NPC. (C) The FG domain of Nup42 recruits the mRNP in close proximity to Dbp5, and Dbp5-ATP binds RNA. Dbp5 might also be a constituent of the exporting mRNP. (D) ATP hydrolysis induces a conformational change in Dbp5 and the bound RNA for release of Nab2, and Mex67-Mtr2, which are recycled into the nucleus for additional rounds of mRNP export. The remodeled mRNP is released into the cytoplasm. Dbp5 interacts with the Nup159 amino terminal domain (NTD) to facilitate ADP release.